Motions of a Rimless Spoked Wheel: a Simple 3D System with Impacts

Michael J. Coleman Anindya Chatterjee[1] Andy Ruina

Department of Theoretical and Applied Mechanics

Cornell University, Ithaca, NY 14853-7501 USA

Accepted for publication in Dynamics and Stability of Systems

Original submission date: August 1, 1996

modified: April 29, 1997

[1]current address: Engineering Science and Mechanics, 227 Hammond Bldg, Penn State University, Ur Park, PA 16802

Abstract

This paper discusses the mechanics of a rigid rimless spoked wheel, or regular polygon, 'rolling' downhill. By *rolling*, we mean motions in which the wheel pivots on one 'support' spoke until another spoke collides with the ground, followed by transfer of support to that spoke, and so on. We carry out three-dimensional numerical and analytical stability studies of steady motions of this system. At any fixed, large enough slope, the system has a one-parameter family of stable steady rolling motions. We find analytic approximations for the minimum required slope at a given heading for stable rolling in three dimensions, for the case of many spokes and small slope. The rimless wheel shares some qualitative features with passive-dynamic walking machines; it is a passive three dimensional system with intermittent impacts and periodic motions. In terms of complexity it lies between one dimensional impact oscillators and three dimensional walking machines. In contrast to a rolling disk on a flat surface which has steady rolling motions that are only *neutrally* stable at best, the rimless wheel can have asymptotic stability. In the limit as the number of spokes `n` approaches infinity, the behavior of the rimless wheel approaches that of a rolling disk in an averaged sense and becomes neutrally stable. Also, in this averaged sense, the piecewise holonomic system (rimless wheel) approaches a nonholonomic system (disk).

1 Introduction

We study the three dimensional motions of a spoked, rimless wheel 'rolling' down a slope under the action of gravity (see Figure 1). A planar rimless wheel of mass m , with moment of inertia matrix $\mathbf{I}^C$ about the center of mass, and n evenly spaced identical spokes of length ' rolls down a slope of angle fi. The orientation variables are 3-1-2 Euler angles representing pitch( ), heading(`), and bank(^). For 2D motions of the wheel at any fixed heading `, the only non-constant variable is since the motion is then confined to a vertical plane aligned with gravity (^ a constant).

By *rolling*, we mean motions in which the wheel pivots on one 'support' spoke until another spoke collides with the ground, followed by transfer of support to that spoke, and so on.

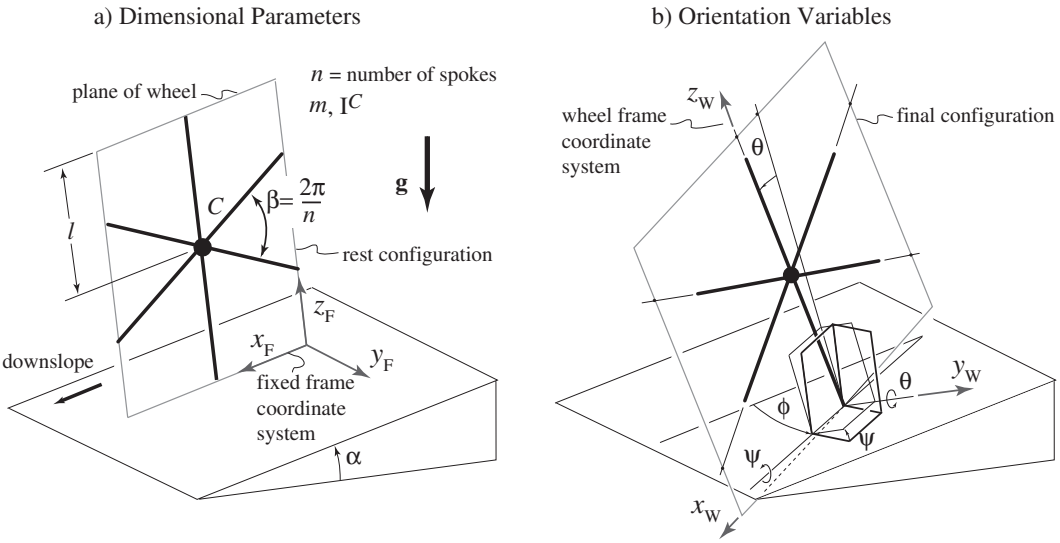

Figure 1: (a) Parameters and (b) orientation variables of the 3D rimless wheel model.

1.1 Motivation

Our interest in the rimless wheel starts from an interest in the dynamics of human walking. Studies of the dynamics of walking motions sometimes involve mechanical systems with the following characteristics: **(a)** over certain periods, the systems have smooth motions that may be roughly described as unstable falling (near a statically unstable configuration); **(b)** these smooth motions are interrupted by collisions, at which velocities change quickly; and support might be transferred from one foot to another; and **(c)** after each collision, another phase of smooth motion begins.

Steady walking corresponds to periodic motions of these dynamic systems. Such systems have been studied with no actuation and control (McGeer, 1990, 1991 [15, 16, 17]; McMahon, 1984 [18]; Garcia, *et. al.*, 1997 [6]; Goswami, *et. al.*, 1996 [7]) as well as with various amounts and types of power input and

active control (see, *e.g.*, Hemami and Chen, 1984 [11]; Furusho and Sano, 1990 [5]; Taga, 1991 [23]; Beletskii, 1990 [1]; Pandy and Berme, 1988 [19]; Hurmuzlu, 1993 [12, 13]; Yamaguchi, 1990 [25]; Zajac and Winters, 1990 [26]; Vukobratovic, *et. al.*, 1990 [24]).

One goal of studies of gait is to understand stability. McGeer's machines, and the walking toys that inspired them (McGeer, 1989) [14], are passive *and* dynamically stable. We are not aware of studies of systems that are simpler than McGeer's, yet retain the essential features mentioned above. Besides wobbling toys with low mass-centers and broad feet (McGeer, 1989) [14], passive dynamic walking machines that are stable in three dimensions have not yet been discovered in theory, simulation or experiment.

Two dimensional motions of the rimless wheel were studied briefly by McGeer (note that in 2D motions, the system has only one degree of freedom). Although three-dimensional motions of a rolling regular polygon (the same as a rimless wheel) were studied by Goyal (1992) [8], three dimensional stability analyses of rolling polygons have not been conducted before. We hope that a 3D stability analysis of the wheel will provide some insight into possible stabilizing mechanisms which in turn might improve our understanding of the dynamics of passive walking in 3D. Like McGeer's walking machines, the rimless wheel has periodic motions in two dimensions which are stable if restricted to two dimensions. Also, like walking machines, the rimless wheel can fall down in 3D. The wheel is simpler to study than the walking machines for the following reasons: **(a)** if the slope is large enough, periodic motions always exist within some interval of heading angle $\grave{}$; **(b)** if periodic motions exist, they are always stable if constrained to 2D; and **(c)** the motion is simpler because the system consists of a single rigid body, unlike the walking machines, which are made of interconnected rigid bodies.

Another reason why the rimless wheel is of interest is that its rolling motion resembles that of a disk, especially so as the number of spokes becomes large. Steady rolling of a disk on a level surface is not asymptotically stable; if slightly disturbed, the wheel wobbles forever (e.g., see Greenwood [9]). The similarity of the rolling motions leads to the question of whether steady motions of the rimless wheel can be asymptotically stable.

2 Description of the System

A wheel of net mass m with the rim removed, and with n evenly spaced identical spokes of length $\grave{}$, rolls down a slope of angle fi (see Figure 1). Assuming n-fold symmetry and that all mass is in the plane, the moment of inertia matrix about the center of mass with the y-axis normal to the plane of the wheel is

$$\mathbf{I}^{C} = \begin{bmatrix} D & 0 & 0 \\ 0 & 2D & 0 \\ 0 & 0 & D \end{bmatrix}; \text{ for some } D > 0: \tag{1}$$

Unlike a wheel with a rim, since this device loses energy at collisions, it cannot roll steadily on a level surface. Here, we only consider downhill rolling.

It is possible that appreciably elastic and/or sliding collisions will make the dynamics of the system more complicated, and perhaps change its stability. We do not consider such cases here. Once a spoke contacts the ground, we assume that it pivots about the contact point until the next spoke collides and we do not allow slip and/or loss of contact between collisions.

The perfectly plastic, instantaneous collision assumption is reasonable when the distance of rebound or sliding is small compared to the distance between neighboring spoke tips, and the time of collisional interaction is small compared to the time between collisions. The perfectly plastic assumption also reduces nicely to the rolling disk as `n ! 1` .

Configuration and State Spaces

We characterize the configuration of the wheel between collisions using 3-1-2 Euler angles as shown in Figure 1. The heading angle is the rotation ` about the original `z` axis, the bank angle is the rotation ^ about the new `x` axis, and the pitch angle is the rotation about the newest `y` axis.

Globally, the system has five generalized coordinates, like a rolling disk: two for contact position and three for the three-dimensional orientation. Unlike the rolling disk, the contact point is stationary between collisions and shifts discontinuously during collisions.

In our stability analysis, we do not keep track of the foot contact position over several foot collisions; we just keep track of the orientation variables `, ^, and . We use equations of motion for a rimless wheel pivoting on one spoke (holonomic system with three degrees of freedom), and use angular momentum-balance-deduced jump conditions to map the state variables from just before a foot collision to just after. Thus, in our analysis, the state space is six dimensional and $\mathbf{q}$, the state vector, is defined to be

$$\mathbf{q} = \begin{bmatrix} \grave{} & \hat{} & \dot{\grave{}} & \dot{\hat{}} & \dot{} \end{bmatrix}^{T} : \tag{2}$$

3 Governing Equations

A *cycle* of the wheel is the motion from one spoke collision through the next. A schematic of one cycle, for downhill rolling, is shown in Figure 2. The beginning and end of the cycle is determined by the pitch angle . The pitch angle of the wheel *between collisions* is restricted to the interval $[-\alpha, \alpha)$ by resetting the pitch angle after each downhill collision to $= -\alpha$.

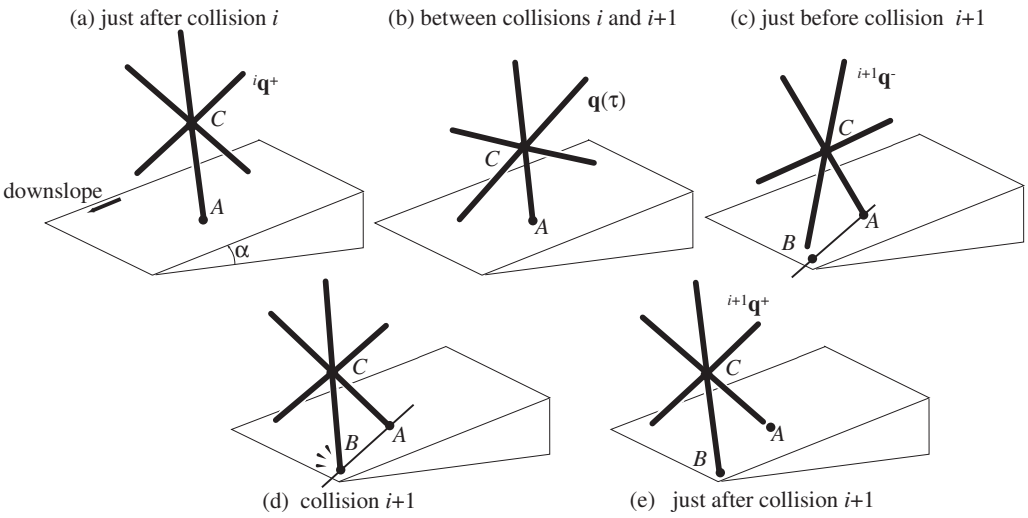

Figure 2: Schematic over one cycle of motion showing: (a) the state of the wheel just after collision i with point A, (b) the state of the wheel between collisions, (c) the state of the wheel just before collision i+1 at point B, (d) collision i+1 at point B, and (e) the state of the wheel just after collision i+1 at point B.

3.1 Equations of Motion between Collisions

Referring to Figure 2, angular momentum balance about the contact point of the spoke currently touching the ground yields the following three non-dimensionalized equations for motion between collisions:

$$\begin{aligned}
\text{sfi c c` ¡ sfi s s^ s` + s c^ cfi} &= \frac{1}{,^2}(\text{c^ ^·· + s^ ·· + ¨}) + \\
&\quad (\text{c c^ ·` + s ·^})(\text{¡ s c^ ·` + c ·^}) \\
0 &= \text{h s c^ ·^ ¡ c s^ ^·· + c c^ ¨ + c ·^ + s ^¨ +} \\
&\quad (\text{s^ ·` + ·})(\text{¡ s c^ ·` + c ·^})\text{i} \\
\text{c^ s` sfi + s^ cfi} &= \text{¡}\frac{1+,^2}{2,^2}\text{h c c^ ·` ¡ s s^ ^·· + s c^ ¨ + s ·^ ¡ c ^¨ +} \\
&\quad (\text{s^ ·` + ·})(\text{c c^ ·` + s ·^})\text{i}
\end{aligned} \tag{3}$$

where 's'and 'c' are used to denote 'sin' and 'cos', and $,^2 \cdot \frac{1}{2\text{J}+1}$ with the square of the radius of gyration $\text{J} \cdot \frac{\text{D}}{\text{m}\,\text{`}^2}$ (non-dimensionalized with respect to `). An overdot indicates differentiation with respect to non-dimensional time ¿ $\cdot \sqrt{\text{g=`}}$ These equations are simply those of an inverted rigid body pendulum. This set of equations can be converted to a first order system of the form $\dot{\mathbf{q}} = \mathbf{g}(\mathbf{q};\mathbf{p});$ where $\mathbf{p}$ is a vector of the parameters, $\mathbf{p} = (,^2; \text{fi})$: We do not restate the equations in first order form for brevity. Henceforth, the dependence on the parameters $\mathbf{p}$ will not be explicitly stated.

As a brief aside, the parameter fi could be eliminated from the equations of motion by a change of variable using angles measured with with respect to a fixed frame whose z-axis is aligned with gravity rather than

the normal to the plane. By including fi here in equation (3), we eliminate it from the collision transition equations that we develop below.

3.2 Collision Transition Conditions

3.2.1 Collision Rule for Configuration Variables

Due to our choice of Euler angles, the heading and bank angles do not change through a collision. The pitch angle is reset at each collision as support is transferred from one spoke to the next according to the following mapping:

$$7!\ ¡\quad \text{or}\ ^{i\ +} = ¡\ ^{i\ ¡}: \tag{4}$$

Thus, we can write

$$\begin{matrix} 8 & & 9 \\ \gg & `+ & \gg \\ \ll & & \ll \\ & ^{\wedge}+ & \\ \gg & & \gg \\ \cdot & + & ; \end{matrix} = \mathbf{S} \begin{matrix} 8 & & 9 \\ \gg & `¡ & \gg \\ \ll & & \ll \\ & ^{\wedge}¡ & \\ \gg & & \gg \\ \cdot & ¡ & ; \end{matrix} ;\ \text{where}\ \mathbf{S} = \begin{matrix} 2 & & & 3 \\ & 1 & 0 & 0 \\ 6 & & & 7 \\ 6 & & & 7 \\ 6 & 0 & 1 & 0 \\ 7 & & & 7 \\ 7 & & & 7 \\ 4 & & & 5 \\ & 0 & 0 & ¡1 \end{matrix}: \tag{5}$$

3.2.2 Collision Rule for Angular Rates

We model the collision as instantaneous. When a spoke collides with the ground, we assume that the trailing spoke instantaneously loses contact with the ground so that only one spoke is in contact with the ground at any time. We assume that no impulse is transmitted at the trailing spoke and that the collision of the new spoke with the ground is perfectly plastic. Under these assumptions, the angular rates just before and after a collision are related as follows:

$$\begin{matrix} 8 & & 9 \\ \gg & \dot{`}+ & \gg \\ \ll & & \ll \\ & \dot{^{\wedge}}+ & \\ \gg & & \gg \\ \cdot & \cdot + & ; \end{matrix} = \mathbf{T} \begin{matrix} 8 & & 9 \\ \gg & \dot{`}¡ & \gg \\ \ll & & \ll \\ & \dot{^{\wedge}}¡ & \\ \gg & & \gg \\ \cdot & \cdot ¡ & ; \end{matrix} ;\ \text{where}\ \mathbf{T} = \begin{matrix} 2 & & & 3 \\ & 1 + \frac{2,^2}{1+,^2}(\cos\frac{2\ldots}{n}\ ¡\ 1) & 0 & 0 \\ 6 & & & 7 \\ 6 & & & 7 \\ 6 & ¡\ \frac{,^2}{1+,^2}\cos\hat{}\ \sin(\frac{2\ldots}{n}) & 1 & 0 \\ 6 & & & 7 \\ 6 & & & 7 \\ 6 & 2,^2\frac{1¡,^2}{1+,^2}\sin\hat{}\ \sin^2(\frac{\ldots}{n}) & 0 & 1 + ,^2(\cos\frac{2\ldots}{n}\ ¡\ 1) \\ 4 & & & 5 \end{matrix}: \tag{6}$$

The (3;3) element of the matrix **T** appears again in the stability calculations. We call it „ · $1+,^2(\cos\frac{2\ldots}{n}\ ¡\ 1)$.

3.2.3 Total Collision Rule

Finally, we can merge the transition rules for the orientation variables and their rates into one map from the state of the system just before a collision to just after:

$$\begin{pmatrix} \gamma^+ \\ \alpha^+ \\ \theta^+ \\ \dot{\gamma}^+ \\ \dot{\alpha}^+ \\ \dot{\theta}^+ \end{pmatrix} = \mathbf{L} \begin{pmatrix} \gamma^- \\ \alpha^- \\ \theta^- \\ \dot{\gamma}^- \\ \dot{\alpha}^- \\ \dot{\theta}^- \end{pmatrix}; \text{ where } \mathbf{L} = \begin{bmatrix} \mathbf{S} & 0 \\ 0 & \mathbf{T} \end{bmatrix}: \tag{7}$$

We can rewrite this collision law that maps the state of the wheel just before to just after a collision as

$$\mathbf{q}^+ = \mathbf{h}(\mathbf{q}^-) = \left(\mathbf{L}(\mathbf{q}^-)\right) \mathbf{q}^-; \tag{8}$$

where the matrix $[\mathbf{L}(\mathbf{q}^-)]$ depends only on the orientation variables and not their rates.

4 Poincaré Section, Return Map, and Fixed Points

To study this system, we use a Poincaré section. Ignoring the absolute position of the wheel on the plane, the rimless wheel has a six-dimensional phase space with coordinates $(\gamma; \alpha; \theta; \dot{\gamma}; \dot{\alpha}; \dot{\theta})$. Instead of taking a Poincaré section at fixed intervals of time, a natural place to sample this space is at the points of discontinuity, the collisions, where we know the pitch angle of the wheel to be $\theta = \frac{\pi}{n}$. The map we use, say $\mathbf{f}$, takes the state of the wheel from just after one collision to just after the next collision.

This mapping approach has also been used in other work involving discontinuous vector fields such as studies of: hopping robots (Bühler and Koditschek, 1990 [3]); bouncing balls (Guckenheimer and Holmes, 1983 [10]); elasto-plastic oscillators (Pratap, *et. al.*, 1992 [20]); impact oscillators (Shaw and Holmes, 1983 [21], Shaw and Rand, 1989 [22]); and walking (McGeer, 1991 [17], Hurmuzlu, 1993 [12, 13]). [1]

Note that the Poincaré section is taken at the same θ for every collision; thus, we assume that the surface of the slope is not curved or bumpy so that the wheel must rotate through the same angle $2\alpha = \frac{2\pi}{n}$ between collisions; thus, the Poincaré section is taken at the same θ for every collision.

The state of the system *after* each collision is a point on the Poincaré section. The map from one point to the next can be written as $\mathbf{q} \mapsto \mathbf{f}(\mathbf{q})$ or

$$^{i+1}\mathbf{q}^+ = \mathbf{f}(^{i}\mathbf{q}^+); \tag{9}$$

[1] A general discussion of the dynamics of systems with impacts can be found in Brogliato, 1996 [2].

where we call $\mathbf{f}$ the *return map* (or Poincaré map) and ${}^{i}\mathbf{q}^{+}$ is the state vector of the system at the start of a cycle, just after the i_{th} collision.

The map $\mathbf{f}$ may be looked upon as a composition of two maps, $\mathbf{f} = \mathbf{h}-\mathbf{d}$; here, $\mathbf{d}$ governs the motion from just after collision i to just before collision $i+1$, obtained by integrating the equations of motion between collisions, and $\mathbf{h}$ governs support transfer, from just before to just after collision $i+1$.

For periodic or steady motion, we must find fixed points of the return map, $\mathbf{q}^{\prime} = \mathbf{f}(\mathbf{q}^{\prime})$.

5 Stability of Periodic Motions

In this paper we consider a system that, with fixed system parameters, (m, n, $\backprime$, J), exhibits a one-parameter family of periodic motions corresponding to rolling down the slope at different headings. On a Poincaré section, periodic motions appear as fixed points; thus a 1 parameter family of periodic motions appears as a curve on the Poincaré section.

If Σ is the Poincaré section, the return map is a function of $\mathbf{q} \in \Sigma$, given by $\mathbf{q}_{n+1} = \mathbf{f}(\mathbf{q}_n)$. For any trajectory of the system, given an initial intersection with the Poincaré section, $\mathbf{q}_0$, the return map generates a sequence of iterates, $\mathbf{q}_1, \mathbf{q}_2, \mathbf{q}_3, \ldots$ Any $\mathbf{q}$ for which $\mathbf{f}(\mathbf{q}^{\prime}) = \mathbf{q}^{\prime}$ is a fixed point on the Poincaré section.

Definitions: We use the following definitions of stability. Let $\mathbf{q}^{\prime} \in \Sigma$ be a fixed point. The fixed point $\mathbf{q}^{\prime}$ is *stable* if, for any $\varepsilon > 0$, there exists $\delta > 0$ such that whenever $\|\mathbf{q}_0 - \mathbf{q}^{\prime}\| < \delta$, $\|\mathbf{q}_n - \mathbf{q}^{\prime}\| < \varepsilon$ for all positive n. The fixed point $\mathbf{q}^{\prime}$ is *asymptotically stable* if, in particular, there exists $\delta > 0$ such that whenever $\|\mathbf{q}_0 - \mathbf{q}^{\prime}\| < \delta$, $\|\mathbf{q}_n - \mathbf{q}^{\prime}\| < \varepsilon$ for all positive n and $\lim_{n \to \infty} \mathbf{q}_n = \bar{\mathbf{q}}^{\prime}$ exists. Note that we do not insist that $\bar{\mathbf{q}}^{\prime} = \mathbf{q}^{\prime}$, only that $\|\bar{\mathbf{q}}^{\prime} - \mathbf{q}^{\prime}\| < \varepsilon$, and therefore our use of the term asymptotic stability is less restrictive than usual. Clearly, if $\bar{\mathbf{q}}^{\prime}$ exists, it must be a fixed point. Thus, we call a periodic motion asymptotically stable if, when slightly disturbed from this motion, the system asymptotically approaches some *nearby* periodic motion. This is the strongest type of stability possible when there is a family of periodic motions, since the perturbed point $\mathbf{q}_0$ could just as well be a perturbation of $\bar{\mathbf{q}}^{\prime}$ as a perturbation of $\mathbf{q}^{\prime}$.

Calculations: In stability calculations, we first compute a fixed point of interest, say $\mathbf{q}^{\prime} \in \Sigma$. Then we select some perturbed point $\mathbf{q}_0$ which lies close to $\mathbf{q}^{\prime}$. Numerically or analytically, we find the next iterate $\mathbf{q}_1 = \mathbf{f}(\mathbf{q}_0)$. To a linear approximation, $\mathbf{q}_1 = \mathbf{q}^{\prime} + \mathbf{J}(\mathbf{q}_0 - \mathbf{q}^{\prime})$, where $\mathbf{J}$ is the Jacobian of the map, evaluated at $\mathbf{q}^{\prime}$. If the eigenvalues of the Jacobian are all smaller than one in magnitude, then the fixed point is asymptotically stable in the traditional sense. Since we have a one-parameter family of fixed points, one eigenvalue will always be exactly equal to one. If all the *other* eigenvalues are smaller than one in magnitude, then the fixed point is asymptotically stable in the weak sense described above.

For the system we consider in this paper, the Poincaré section is five dimensional (the phase space is six dimensional). Thus, the Jacobian is a 5×5 matrix which can be numerically computed by five calculations

using independent perturbations $\mathbf{q}_0 \; ; \; \mathbf{q}'$ for each case. Naturally, the perturbed point $\mathbf{q}_0$ must lie *on* the Poincaré section in each case. In our calculations, we chose to do *six* (dimension of the phase space) calculations, where the perturbed point $\mathbf{q}_0$ *need not* lie on the Poincaré section in each case, resulting in a 6×6 Jacobian matrix. **Note:** Our six dimensional calculation yields a Jacobian with six eigenvalues; one eigenvalue is exactly zero, and reflects the fact that the initially perturbed point might lie off the Poincaré section, but the next iterate $\mathbf{q}_1$ will lie exactly on the Poincaré section. The remaining five eigenvalues of our 6×6 Jacobian matrix are identical to the eigenvalues of the 5×5 Jacobian obtained by selecting initial perturbations only on the Poincaré section. Since our system has a one-parameter family of fixed points, one eigenvalue is exactly equal to one. Thus, there remain four eigenvalues to be examined.

6 Motion Restricted to 2D: Some Results

A detailed analysis of all possible 2D motions of the rimless wheel may be found in Coleman (1997) [4]. A simple analysis is described in McGeer (1990) [15]. Here, we consider only the motions near steady downhill rolling motions.

If the rimless wheel completes a downhill cycle, the kinetic energy of the wheel at the end-of-cycle, just before collision $i+1$, is greater than the kinetic energy at the start-of-cycle, just after collision i, due to the downhill slope ($KE_{i+1}^{-} > KE_{i}^{+}$). The kinetic energy of the wheel drops instantaneously at impact. For downhill motions, only three outcomes are possible when **(a)** the slope is big enough and **(b)** the wheel has enough initial kinetic energy make it past the vertical position in its cycle of motion to the next downhill collision. These possibilities are:

1. Periodic motion occurs; this happens if the energy lost in collision is exactly balanced by the kinetic energy gained in falling. In this case, the state variables are equal to those at the start of the previous cycle. The wheel is in periodic or limit cycle motion that repeats indefinitely.

2. The wheel slows down towards a periodic motion, which may be shown to be unique; this happens if more energy is lost in collision than gained in moving downhill.

3. The wheel speeds up towards the periodic motion; this happens if more energy is gained in moving downhill than lost in collision.

In Coleman (1997) [4], it is shown that condition **(a)** is satisfied if the effective slope angle $\quad > \quad_c$ where $\quad_c$ satisfies

$$1 \; ; \; \cos\frac{\cdots}{n}\cos \quad_c \; ; \; \frac{1+\;''^{2}}{1 \; ; \;''^{2}}\sin\frac{\cdots}{n}\sin \quad_c = 0; \tag{10}$$

and that condition **(b)** is satisfied if the the pitch rate just after a collision $\dot{\theta}^+ > \dot{\theta}_c$ where $\dot{\theta}_c$ is given by

$$\dot{\theta}_c = \sqrt{2g/R(1 - \cos(\alpha - \frac{\pi}{n}))}. \tag{11}$$

Based on the observations above, key aspects of the 2D motions that are relevant to steady rolling motions in 3D are stated below:

1. For large enough slopes, $\alpha > \alpha_c$, unique steady 2D rolling motions *always exist.*
2. The steady 2D motions (restricted to 2D) are asymptotically stable. The eigenvalue of the linearization of the map about the fixed point is $\rho^2 < 1$.

7 3D Motions

The solutions found in 2D will satisfy the 3D equations of motion; i.e., all 2D solutions are also 3D solutions. There is a family of 2D periodic motions restricted to different vertical planes; i.e., the wheel may roll downhill at different heading angles ψ. We call these steady 3D motions *planar* (or 2D) *limit cycles.* A planar limit cycle is illustrated schematically in Figure 3. Corresponding to each fixed point is a trajectory in

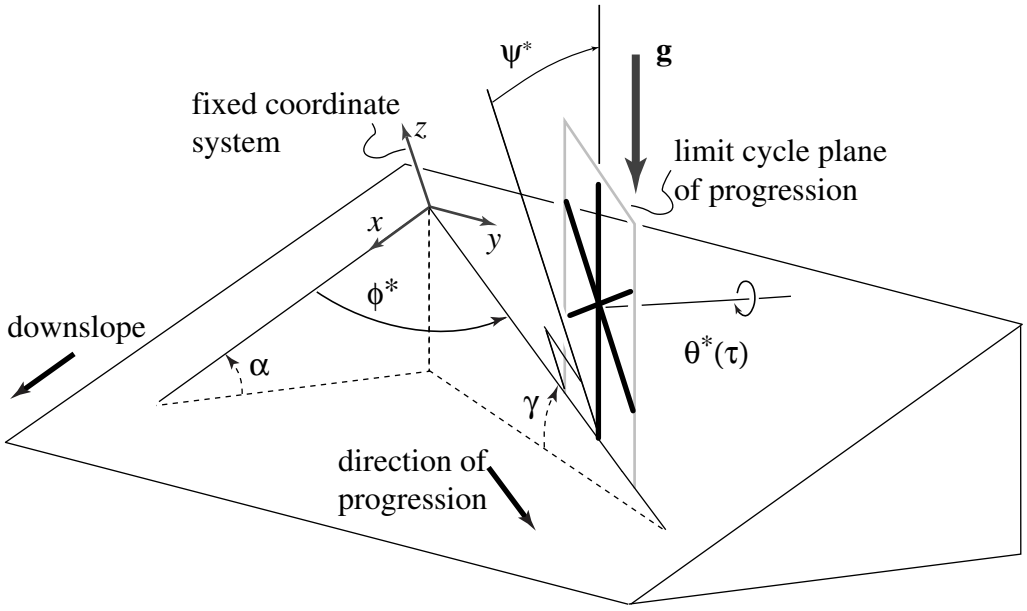

Figure 3: The schematic here depicts the planar limit cycle motion, for the 3D wheel, showing how the plane of the wheel at heading ψ is aligned with the force acting on the wheel due to gravity.

phase space in between collisions. With a slight abuse of notation, we also use an asterisk '*' to denote this trajectory $\mathbf{q}^*(\tau)$, which we call the 2D *limit cycle trajectory* (see Figure 6 in the appendix); we distinguish it from the fixed point $\mathbf{q}^*$ by showing it as a function of the non-dimensional time τ. The fixed point $\mathbf{q}^*$

and its associated 2D limit cycle trajectories between collisions are summarized in Table 1. For motions

Limit Cycle Trajectory (in time)	$\theta'(\tau) = \theta'$	$\dot{\theta}'(\tau) = 0$	$\psi'(\tau) = \psi'$	$\dot{\psi}'(\tau) = 0$	$\phi'(\tau)$	$\dot{\phi}'(\tau)$
Fixed Point of $\mathbf{f}$ (on Σ)	θ'	$\dot{\theta}' = 0$	$\psi' \cdot \psi'(\theta'; \gamma)$	$\dot{\psi}' = 0$	$\phi' = -\frac{\pi}{n}$	$\dot{\phi}' \cdot \dot{\phi}'(\gamma; n; \mu)$

Table 1: The planar limit cycle in three dimensions. The limit cycle time histories $\theta'(\tau)$, $\dot{\theta}'(\tau)$, $\psi'(\tau)$, and $\dot{\psi}'(\tau)$ are constant over a cycle and equal to the corresponding fixed point values at the start-of-cycle. The limit cycle pitch angle $\phi'(\tau)$ and rate $\dot{\phi}'(\tau)$ are not constant.

of the wheel restricted to two dimensions,the plane of the wheel is parallel to the line of action of the net gravity force acting on the wheel. In terms of the 3D variables, this gives the bank angle ψ' of the wheel as a function of the slope angle fi and the heading angle θ'

$$\psi' \cdot \psi(\theta'; \text{fi}) = \tan^{-1}(-\sin\theta' \tan\text{fi}): \tag{12}$$

The effective slope γ at a particular heading is given by

$$\gamma \cdot \gamma(\theta') = \sin^{-1}(\sin\text{fi}\ \cos\theta'): \tag{13}$$

The heading angle θ' may be looked upon as a free parameter that determines a one-parameter family of steady rolling motions. Finally, the *limit cycle pitch rate*, as sampled on the Poincaré section, and the *limit cycle period* τ' are, respectively,

$$\dot{\phi}' \cdot \dot{\phi}'(\gamma; n; \mu) = \sqrt{\frac{4\mu^2 - 2\sin\frac{\pi}{n}\sin\gamma}{1-\mu^2}} \text{ and} \tag{14}$$

$$\tau' \cdot \tau'(\gamma; n; \mu) = \int_{-\frac{\pi}{n}}^{\frac{\pi}{n}} \frac{d\phi}{\sqrt{(\dot{\phi}')^2 + 2\mu^2(\cos(\frac{\pi}{n}) - \cos\gamma)}}: \tag{15}$$

both of which can be found using a simple 2D energy analysis. As the number of spokes n gets large, various planar limit cycle quantities (the limit cycle pitch rate $\dot{\phi}'$, the limit cycle time between collisions τ', the critical effective slope angle γ_c, and the collision parameter μ) scale with n as follows:

$$\dot{\phi}' \sim \sqrt{\frac{n\sin\gamma}{\pi}}; \quad \tau' \sim \frac{2(\frac{\pi}{n})^{\frac{3}{2}}}{\sqrt{\sin\gamma}}; \quad \gamma_c \sim \frac{2\pi^3}{n^3}; \quad \text{and } \mu \sim 1 - 4\frac{\pi^2}{n^2}: \tag{16}$$

Here, γ_c is the minimum required slope for steady rolling motions to exist. The limit cycle pitch angle, equal to half the angle between the spokes, is $\phi' = -\pi/n$ which obviously scales as $\phi' \gg O(1/n)$.

For our 3D analytical stability study, we take the slope angle fi to be inversely proportional to the number of spokes, $\mathrm{fi} = \frac{\mathrm{fi}}{\mathrm{n}}$, which implies for any heading ` that

$$= \frac{\bar{}}{\mathrm{n}} + \mathrm{O}\left(\frac{1}{\mathrm{n}^3}\right) \qquad {}_{\mathrm{c}} \gg \mathrm{O}\left(\frac{1}{\mathrm{n}^3}\right) \tag{17}$$

where $\bar{} \gg \mathrm{O}(1)$ is a constant. For such slopes, the limit cycle period scales as ¿´ » O(1=n) and the limit cycle pitch rate tends to a constant ˙´ , $\frac{\mathrm{p}}{\bar{}=\ldots}$ As n ! 1 , we obtain a disk on a flat surface rolling at constant speed proportional to $\mathrm{p}=$.

8 3D Stability of the 2D Limit Cycle

For a rimless wheel restricted to planar motions, asymptotically stable fixed points exist if the effective slope is big enough. The limit cycle pitch rate ˙´ is a function of the number of spokes, the radius of gyration of the wheel, and the effective slope angle. We determine the three-dimensional stability of this planar limit cycle whose 2D characteristics we already know in closed form from a nonlinear analysis of the rimless wheel restricted to two dimensions, as summarized in the previous section (for details, see Coleman (1997) [4]).

In this paper, we focus on the three-dimensional stability of the planar limit cycle. Though the 3D rimless wheel may have other periodic motions other than 2D limit cycles, such as zig-zagging or looping motions, we did not look for these solutions or investigate their stability.

Unlike the 2D case, we cannot find explicitly the 3D return map, its non-planar fixed points, or the stability of fixed points. Instead, we approximate the Jacobian of the map at the planar fixed point both numerically and analytically. In the analytical approach, the approximation is based on a perturbation expansion for a wheel with many spokes and small slopes. (See Appendix for details.)

8.1 Numerical Approximation

Figure 4 shows the state of the rimless wheel disturbed slightly from a planar limit cycle over many collisions. For the parameter values used, the steady rolling motion is stable. The disturbance eventually decays and the rimless wheel enters into a new planar limit cycle at a slightly different heading (and corresponding bank angle) across the slope. The six numerically evaluated eigenvalues[2] for the case in Figure 4 are: ${}_0 = 0$, ${}_1 = 1$ (see discussion in Section 5), ${}_2 = 0{:}9011$, ${}_{3;4} = 0{:}9108$§ $0{:}3839\mathrm{i} = 0{:}9884\, \mathrm{e}^{\S\, 0{:}3989\mathrm{i}}$, and ${}_5 = 0{:}9613$. We will compare these numerical results for this case to asymptotic estimates in a later section. Since j j • 1, and only one eigenvalue is exactly equal to one, the planar limit cycle motion is asymptotically stable.

[2] The equations were integrated and the Jacobian evaluated numerically, using MATLAB. The numerically computed J bianJ is not reproduced here due to limitations of space.

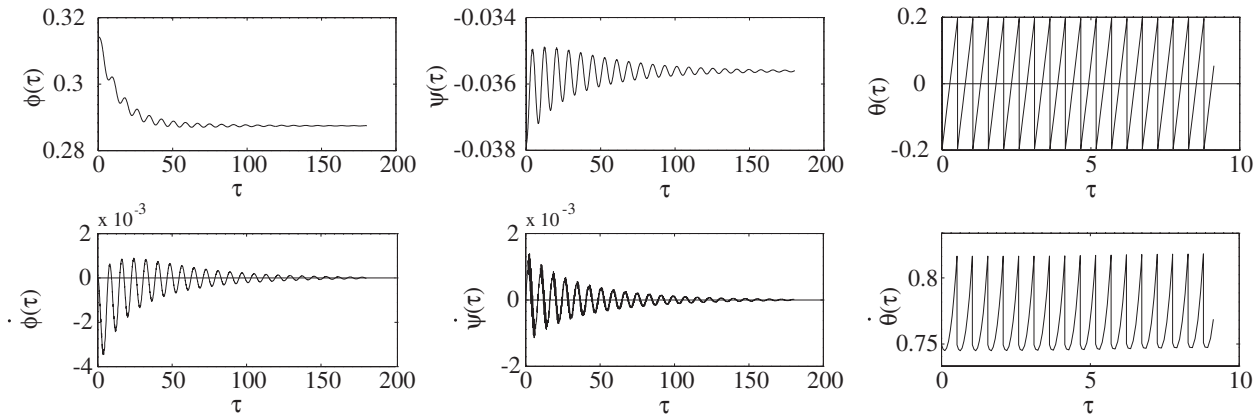

Figure 4: State of the rimless wheel plotted versus ¿ for 350 collisions after it is perturbed from its limit cycle with a disturbance in the bank angle $\Delta\hat{}_0 = 0.001$. For this simulation, $2J = 0.5$ (or $,^2 = \frac{2}{3}$), n = 16, fi = 2=n, and $\grave{}_0 = \ldots=10$. Note that and $\dot{}$ are plotted over only about 17 collisions since their variation with ¿ is at too high a frequency to be usefully displayed over 350 collisions. The discontinuities in the graphs of angular rates are due to the collisions while the discontinuities in the graph of (¿) are due to resetting from $\frac{\cdots}{n}$ to ¡ $\frac{\cdots}{n}$ at collisions.

Given the initial perturbed state of the wheel from its limit cycle, we can predict approximately the subsequent motion of the wheel, using **J**. We can do this as follows. To the linear approximation, the small initial perturbation to the fixed point of the return map propagates over k collisions as

$$\Delta\mathbf{q}_k = \mathbf{J}^k \, \Delta\mathbf{q}_0 \tag{18}$$

where $\Delta\mathbf{q}_0$ is the perturbation to the fixed point $\mathbf{q}_0'$.

The new limit cycle of the wheel after many collisions is given by

$$\mathbf{q}' = \mathbf{q}_0' + \lim_{k \to \infty} \mathbf{J}^k \Delta\mathbf{q}_0 : \tag{19}$$

In this numerical example,

$$\mathbf{q}_0' = \{\grave{}' = 0.3142;\ \hat{}' = ¡\,0.0378;\ ' = ¡\,0.1963;\ \dot{\grave{}}' = 0;\ \dot{\hat{}}' = 0;\ \dot{}' = 0.7496\}^T$$

and $\Delta\mathbf{q}_0 = \{\Delta\grave{}_0 = 0;\Delta\hat{}_0 = 0.001;\Delta\ _0 = 0;\Delta\dot{\grave{}}_0 = 0;\Delta\dot{\hat{}} = 0;\Delta\dot{} = 0\}^T$. Therefore, we estimate the state vector after 350 collisions to be

$$\mathbf{q}_0' + \mathbf{J}^{350}\Delta\mathbf{q}_0 = \{0.2872;\ ¡\,0.0356;\ ¡\,0.1963;\ 0.0000;\ 0.0000;\ 0.7529\}^T : \tag{20}$$

In comparison, we obtained the state vector from numerical integration as

$$\mathbf{q}' = \{0.2875;\ ¡\,0.0356;\ ¡\,0.1963;\ \ 0.0000;\ 0.0000;\ 0.7527\}^T \tag{21}$$

after 350 collisions, rather close agreement as expected.

Also, note that, for the new limit cycle, the numerically calculated heading and bank angles are in the proper relationship and the numerically calculated limit cycle pitch rate is correct for the effective slope at the final heading:

$$\hat{\chi} = \tan^{-1}(-\sin\hat{\chi}\tan\phi) = -0.0356 \text{ and } \dot{\hat{\chi}} = \frac{\sqrt{4\mu^2 r^2 \sin\frac{\pi}{n}\sin}}{1-\mu^2} = 0.7527$$

where r is defined by equation (13).

More qualitatively, we note that the eigenvalues of largest magnitude less than 1 are $\lambda_{3,4}$, whose magnitude is about 0.99. These eigenvalues cause the slow, oscillatory decay in the disturbance. Note that the period of oscillation $2\pi/0.3989$ is about 16, and so there are about 22 oscillations over 350 collisions. After, say, 80 collisions, we have $(\lambda_2)^{80} < 0.0003$, $(\lambda_5)^{80} < 0.05$, and $|\lambda_{3,4}|^{80} \approx 0.39$. Therefore, the decay in the disturbance after about five oscillations (80 collisions) is almost solely governed by $\lambda_{3,4}$, and the decay per oscillation (per 16 collisions) thereafter is roughly given by $|\lambda_{3,4}|^{16} \approx 0.83$, which agrees with Figure 4.

The good agreement between the linearized dynamics (equation (20)) and the numerical solution (equation (21), Figure 4) are an indication that the numerical calculations are sound and the asymptotic stability conclusion is correct.

8.2 Analytical Approximation

In order to analytically determine the 3D stability of the steady rolling motion, we use a perturbation method with $\epsilon = 1/n$ as a small parameter. A numerical study of the eigenvalues of the Jacobian of the map for large n shows that two eigenvalues are approximately of the form $1 + k\epsilon^2$ for some constant k, so the Jacobian needs to be found at least up to $O(\epsilon^2)$.

Our approach is based on the following observations: **(a)** we cannot find an analytical approximation of the full 3D return map; **(b)** we can find an analytical approximation to the steady rolling or periodic motion as a power series in ϵ, up to arbitrary orders; **(c)** we can solve the first order (or linearized) variational equations for motions close to the limit cycle, also up to arbitrary orders in ϵ; and, **(d)** using **(b)** and **(c)**, we can find the Jacobian of the return map at the fixed point up to arbitrary orders in ϵ.

8.2.1 Asymptotic Expansion

We define

$$\epsilon \cdot \frac{1}{n} \tag{22}$$

and note that ϵ is small but finite and, hence, much larger than the variations used in the stability calculations. A detailed description of the perturbation analysis of this problem (carried out using the symbolic computation package MAPLE) may be found in Coleman (1997) [4]. We summarize the analysis below.

We rescale the non-dimensional time ¿, pitch angle , and slope angle as follows:

$$\begin{aligned} ¿ &= \dagger \mathrm{T} \\ (¿) &= \dagger\Theta(\mathrm{T}) \\ \mathrm{fi} &= \dagger\mathrm{fi}: \end{aligned} \tag{23}$$

Using these new scalings, we write the variational equations for small perturbations using

$$\begin{aligned} \grave{}(\mathrm{T}) &\ldots \grave{}' + \dagger\hat{\grave{}}(\mathrm{T}); \\ \hat{}(\mathrm{T}) &\ldots \hat{}' + \dagger\hat{\hat{}}(\mathrm{T}); \text{ and} \\ \Theta(\mathrm{T}) &\ldots \Theta'(\mathrm{T}) + \dagger\hat{\Theta}(\mathrm{T}); \end{aligned} \tag{24}$$

where

$$\hat{}' \cdot \hat{}'(\grave{}';\mathrm{fi}) = \tan^{-1}(¡ \sin\grave{}' \tan(\dagger\mathrm{fi})) \tag{25}$$

and

$$\dagger ¿ \dagger: \tag{26}$$

We need to find the motions of the system up to strictly first order in †. The motions can be found in terms of a power series in †. We expand $\Theta'(\mathrm{T})$ as

$$\Theta'(\mathrm{T}) = \Theta'(\mathrm{T};\dagger) \ldots \Theta_0(\mathrm{T}) + \dagger\Theta_1(\mathrm{T}) + ¢\,¢\,¢ + \dagger^m\,\Theta_m(\mathrm{T}) + ¢\,¢\,¢ \tag{27}$$

Setting $\dagger = 0$ in the newly scaled equations of motion, we get an approximate solution for limit cycle pitch angle $\Theta'(\mathrm{T})$ and limit cycle period T' accurate up to and including $\mathrm{O}(\dagger^3)$ terms

$$\begin{aligned} \Theta'(\mathrm{T}) &= \hat{}\sqrt{\frac{}{}}\,!\,\Big"\sqrt{\frac{}{}}\,\mathrm{T}^3 \\ &\quad + \frac{1}{2},^2(^- ¡ \ldots)\mathrm{T}^2 + \frac{1}{12}\,\hat{}\sqrt{\frac{}{}}(1 ¡ 18,^2) ¡ \frac{\sqrt{5}}{\ldots\cos^2\grave{}'}\,!\,\#\,\mathrm{T}\;\dagger^2 + \mathrm{O}(\dagger^4) \end{aligned} \tag{28}$$

$$\mathrm{T}' = 2\,\pi\sqrt{\frac{\ldots^3}{^-}} + \frac{2}{3}\sqrt{\frac{\ldots^9}{^{-3}}} + \frac{1}{6}\sqrt{\frac{\ldots^7}{^-}}(6,^2 ¡ 1) + \frac{1}{6}\frac{\sqrt{(\ldots^-)^3}}{\cos^2\grave{}'}\,!\,\dagger^2 + \mathrm{O}(\dagger^4) \tag{29}$$

where (see equation (17))

$$^- \cdot \mathrm{fi}\cos\grave{}' : \tag{30}$$

Recall that the equations of motion for the system are of the form $\dot{\mathbf{q}} = \mathbf{g}(\mathbf{q})$. The variational equations have time-varying coefficients which involve $\Theta'(\mathrm{T})$ above,

$$\dot{\hat{\mathbf{q}}}(\mathrm{T}) \,' \,\mathrm{D}\,\mathbf{g}(\mathbf{q}'(\mathrm{T}))\hat{\mathbf{q}}(\mathrm{T}): \tag{31}$$

8.2.2 Eigenvalues of the Approximate Jacobian

Constructing the approximation to the Jacobian evaluated at the fixed point of the return map as described in the appendix, we get the approximation to the eigenvalues of the Jacobian as

$$\begin{aligned}
\lambda_0 &= 0 \\
\lambda_1 &= 1 + O(\epsilon^3) \qquad \text{(in fact, this eigenvalue is exactly 1)} \\
\lambda_2 &\approx 1 - (4\alpha^2\beta^2)\epsilon^2 \approx \mu^2 < 1 \\
\lambda_{3,4} &\approx 1 \pm \mathrm{fl}_0\epsilon + \mathrm{fl}_1\epsilon^2 \\
\lambda_5 &\approx 1 - \mathrm{fl}_2\epsilon^2
\end{aligned} \tag{32}$$

where

$$\begin{aligned}
\mathrm{fl}_0 &= 2\alpha^2\sqrt{\frac{\alpha^2\beta^2 - 2^-}{^-(1+\beta^2)}}; \\
\mathrm{fl}_1 &= \frac{2(-^{-2}\beta^4 + 2\alpha^2\beta^4 - 8\alpha^2\beta^{2-} + ^{-2}\beta^2 + 8^{-2})\alpha^2}{^-(\alpha^2\beta^2 - 2^-)(1+\beta^2)}; \text{ and} \\
\mathrm{fl}_2 &= \frac{4(\alpha^2\beta^2 - \beta^{2-} - ^-)\alpha^2\beta^2}{(\alpha^2\beta^2 - 2^-)(1+\beta^2)}:
\end{aligned}$$

The numerical and asymptotic estimates of the eigenvalues are compared in Figure 5 and show the convergence to near-perfect agreement as the number of spokes gets large. Note that the approximation is based on the assumption of large n and the expressions for fl_1 and fl_2 show that accurate estimates are not expected for $\alpha^2\beta^2 - 2^-$ close to zero. For the particular case presented in sub-section 8.1, we compare the numerical and asymptotic estimates of the eigenvalues from equations (32) in Table 2 below. In addition, we compare

	λ_0	λ_1	λ_2	$\lambda_{3,4}$	λ_5
Numerical	0	1	0.9011	$0.9884\, e^{\pm 0.3989i}$	0.9613
Asymptotic	0	1	0.8972	$0.9930\, e^{\pm 0.4232i}$	0.9612

Table 2: Comparison of the numerical and perturbation estimates of the limit cycle eigenvalues for the case presented in Section 8.1 where $2J = 0.5$, n = 16, fi = 2=n, and $\grave{}_0 = \alpha=10$. Better agreement is found for larger n (see Figure 5).

the numerical and asymptotic estimates of the non-dimensional limit cycle period from equation (29); the numerically computed value is $\omega = 0.5155$ and the asymptotic estimate is $\omega = \pm T = 0.5203$.

8.2.3 Stability Criteria

The eigenvalues of the Jacobian of the map have the following interpretations:

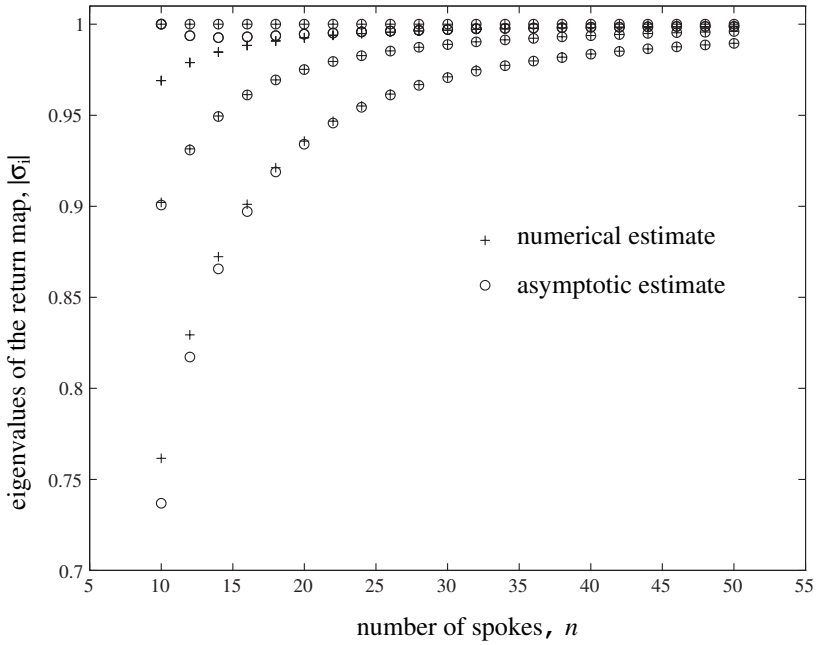

Figure 5: The modulus of the eigenvalues j jof the Jacobian evaluated at the fixed point of the return map are shown for different n, with fi = 2=n, and the arbitrarily chosen values ,^{2} = 2=3, and `$_0$ = ...=10. The zero eigenvalue is not shown.

† $_0$ = 0; and $_1$ = 1 for reasons discussed in Section 5;

† $_2$ ... 1¡ (4,^{2}...^{2})ǂ^2 < 1 comes from the 2D motion; In fact, $_2$ is exactly „^{2}, where „ · 1+,^{2}(cos $\frac{2...}{n}$ ¡ 1); and

† j$_{3;4}$j< 1 and j$_5$j< 1 determine necessary and sufficient conditions for asymptotic stability.

For asymptotic stability of steady planar rolling in 3D (for a wheel of many spokes on a small slope fi and effective slope ' O(ǂ)), from equations (32) we may conclude the following.

1. If fl$_0$ is real, then one of $_{3;4}$ is greater than 1 by an amount O(ǂ). On the other hand, if fl$_0$ is imaginary, then the magnitudes of of $_{3;4}$ as well as $_5$ are 1 + O(ǂ^2) (j$_{3;4}$j ... 1 + $\frac{1}{2}$(2fl$_1$ + ǰfl$_0$ǰ^2)ǂ^2). Therefore, for stability to O(ǂ) we require ...,^{2} ¡ 2$^-$ < 0, or

$$^- > ...,^2=2: \tag{33}$$

2. For stability to O(ǂ^2) we require both **(i)** fl$_2$ > 0 and **(ii)** 2fl$_1$ + ǰfl$_0$ǰ^2 < 0. Condition **(i)** is satisfied if $^-$ > ...,^{2}=(1 + ,^{2}). Note that in this case even equation (33) above is automatically satisfied since ,^{2} = 1=(2J + 1) < 1. Finally, given $^-$ > ...,^{2}=(1 + ,^{2}), condition **(ii)** is automatically satisfied. Therefore, condition **(i)** is both necessary and sufficient to ensure stability, to O(ǂ^2).

So, the asymptotic analysis estimates the condition for asymptotic stability of the planar limit cycle to be

$$^{-} > \ldots, ^{2}=(1 + , ^{2}): \tag{34}$$

Since $^{\cdot}$, the limit cycle pitch rate or rolling speed, is known in terms of $= \dagger^{-}$, the stability results may be expressed in terms of this pitch rate (to lowest order). In terms of limit cycle pitch rate, the two stability criteria (33) and (34) reduce to

$$(^{\cdot})^2 > \frac{, ^2}{2}; \text{ and} \tag{35}$$

$$(^{\cdot})^2 > \frac{, ^2}{1 + , ^2} \tag{36}$$

where, for $0 < , ^2 < 1$, criterion (36) is more stringent than (35) but (35) turns out to be important as discussed below.

8.2.4 Comparison to a Rolling Disk

The criterion on the forward speed for neutral stability of a uniform disk with polar moment of inertia $2J$ rolling in a vertical plane is $(^{\cdot})^2 > , ^2=2$, where $, ^2 = 1=(2J + 1)$ (see e.g., Greenwood, 1965 [9]). This criterion is the same as the $O(\dagger)$ stability criterion (35) above, i.e., fl_0 being imaginary. That the rolling disk criterion and criterion (35) should agree may be seen as follows. If equation (35) is not met for the rimless wheel, i.e., $(^{\cdot})^2 < , ^2=2$ or fl_0 is real, then one eigenvalue takes the form

$$j\ j= 1 + a\dagger; \text{for some real } a > 0: \tag{37}$$

If equation 35 is met, but equation 36 is not necessarily met, then the eigenvalues take the form

$$j\ j= 1 + b\dagger^2; \text{ for some real } b; \text{positive or negative}: \tag{38}$$

As $n ! 1$, the rimless wheel approaches a rolling disk rolling with a constant speed on a level surface; the speed is decided by $^{-}$. In order to compare the rimless wheel and the disk, we examine the propagation of small disturbances not through one spoke collision but rather through one revolution of the wheel at some constant limit cycle pitch rate; i.e., we look at the magnitude of $^{n}_{i}$ as $n ! 1$. We have,

$$\lim_{\dagger ! \ 0} (1 + a\dagger)^{\frac{1}{\dagger}} = e^{a} \text{ and } \lim_{\dagger ! \ 0} \left(1 + b\dagger^2\right)^{\frac{1}{\dagger}} = 1: \tag{39}$$

Thus, it is seen that the $O(\dagger^2)$ stability criterion, equation (36) above, becomes irrelevant in the limit as $n ! 1$ and the associated eigenvalue goes to 1 (from above or below). On the other hand, the $O(\dagger)$ stability criterion, equation (35), predicts instability if fl_0 is real, and neutral stability if fl_0 is imaginary in the limit as $n ! 1$, just like the rolling disk. Therefore, equation (35) governs the stability of the rimless wheel, as $n ! 1$, and agrees with the stability calculations for a rolling disk.

8.3 Aside: Existence of Other Limit Cycles

In the case of 3D motions, if we vary the slope as a parameter for fixed n, then for some slope the eigenvalue λ_5 will be exactly 1. At that particular slope, the eigenvalue 1 has multiplicity two. Therefore, one might expect that at that slope two limit cycles merge.

We do not believe that there are such limit cycles. Our reasoning is as follows. **(a)** As n gets large, the dynamic behavior of the rimless wheel approaches that of a disk on a flat plane (in a suitably averaged sense). Small deviations from pure rolling, for a disk, are limited to small, periodic wobbles. These wobbles occur over a time scale of $O(1)$. For the rimless wheel, this means such wobbles occur over $O(n)$ collisions, which is consistent with the imaginary parts of $\lambda_{3,4}$ being $O(1/n)$. Such 'long-period' motions will not be fixed points of the single-spoke-collision return map we consider. Intuitively, we do not foresee any other types of fixed points of the return map except the one-parameter family of steady rolling motions we have considered. **(b)** Note that fixed points are solutions to the equation $\mathbf{f}(\mathbf{x}) = \mathbf{x}$, or $\mathbf{g}(\mathbf{x}) := \mathbf{f}(\mathbf{x}) - \mathbf{x} = 0$: The Jacobian of the function $\mathbf{g}(\mathbf{x})$ differs from that of $\mathbf{f}(\mathbf{x})$ by the identity, and a double eigenvalue of 1 for $\mathbf{f}$ corresponds to a double-zero eigenvalue for $\mathbf{g}$. However, for another solution branch in addition to the known one-parameter family to appear at that point, the rank of $D\,\mathbf{g}$, the Jacobian of $\mathbf{g}$, should be 4 (2 less than 6). Based on some numerical checks using the singular value decomposition, we believe that (at least typically) the rank of $D\,\mathbf{g}$ is 5 (1 less than 6). In other words, the double eigenvalue has algebraic multiplicity 2 but geometric multiplicity 1. This means that the already known one-parameter family of steady rolling solutions (i.e., limit cycles) is all there is.

9 Conclusions and Future Work

In this paper, we have presented an analysis of a 3D dynamic system with intermittent impacts, that shares some qualitative features with passive dynamic walking machines. A viable computer-algebra based analytical technique for stability studies of systems with intermittent impacts was demonstrated for this moderately complicated system. In another work, this same approach has been successfully used to study the stability of a simple walking machine in 2D (Garcia, *et. al.*, 1996[6]).

A question of general interest to us is the cause of balance stability of 'passive-dynamic' walking machines. Two known mechanisms for asymptotic stability of passive mechanical systems are dissipation and nonholonomic constraints although dissipation can also be destabilizing.

Dissipation: We note that the rimless wheel can be stable when constrained to two dimensions on slopes of $O(1/n^3)$, essentially due to the energy dissipation in collisions. However, the 3D system, with more degrees of freedom, is only stable on slopes of $O(1/n)$. Hence, energy dissipation alone is not sufficient for stability in 3D.

Nonholonomic Constraints: For the rimless wheel, the natural system to compare with is a rolling disk, a classic conservative nonholonomic system. The rolling disk, due to its symmetry with respect to motion reversal, is not asymptotically stable but only neutrally stable. The intermittent collisions are somehow crucial to the asymptotic stability that the rimless wheel has but that the rolling disk does not have. Thus, we do not yet know of a simple heuristic way to explain the asymptotic balance stability of the system studied here.

10 Acknowledgments

The authors thank Saptarsi Haldar for help with numerical work; Jeff Koechling, Mark Myers, Les Schaffer, and Dan Koditschek for useful discussions in the early stages; and Richard Rand for his comments on the final draft of the paper. Coleman was partially funded by a grant from the Whitaker Foundation.

References

[1] V. V. Beletskii. Nonlinear effects in dynamics of controlled two-legged walking. In *Nonlinear Dynamics in Engineering Systems*, pages 17–26, Berlin, 1990. IUTAM, Springer-Verlag. The proceedings are from an IUTAM symposium held in 1989 in Stuttgart, Germany.

[2] Bernard Brogliato. *Nonsmooth Impact Mechanics: Models, Dynamics and Control*. Springer, London, UK, 1996.

[3] M. Bühler and D. E. Koditschek. From stable to chaotic juggling: Theory, simulation, and experiments. In *1990 IEEE International Conference on Robotics and Automation*, pages 1976–1981. IEEE Robotics and Automation Society, IEEE, 1990. The proceedings are from a conference held during May 13-18, 1990 in Cincinnati, Ohio.

[4] M. J. Coleman. *A Stability Study of a Three-dimensional Passive-dynamic Model of Human Gait*. PhD thesis, Cornell University, Ithaca, NY, 1997. in preparation.

[5] J. Furusho and A. Sano. Sensor-based control of a nine-link biped. *The International Journal of Robotics Research*, 9(2), April 1990.

[6] M. Garcia, A. Chatterjee, A. Ruina, and M. J. Coleman. The simplest walking model: Stability, complexity, and scaling. Accepted for publication in The Journal of Biomechanics, 1997.

[7] A. Goswami, B. Thuilot, and B. Espiau. Compass-like biped robot, part I: Stability and bifrucation of passive gaits. Rapport de recherche 2996, Unité de recherche INRIA Rhône-Alpes, St. Martin, France, October 1996.

[8] S. Goyal. personal communication, 1992.

[9] D. T. Greenwood. *Principles of Dynamics*. Prentice Hall, 1965.

[10] J. Guckenheimer and P. Holmes. *Nonlinear Oscillations, Dynamical Systems, and Bifurcations of Vector Fields*. Springer-Verlag, New York, 1983.

[11] H. Hemami and B. Chen. Stability analysis and input design of a two-link planar biped. *The International Journal of Robotics Research*, 3(2):93–101, Summer 1984.

[12] Y. Hurmuzlu. Dynamics of bipedal gait: Part I — objective functions and the contact event of planar five-link biped. *Journal of Applied Mechanics*, 60:331–337, June 1993.

[13] Y. Hurmuzlu. Dynamics of bipedal gait: Part II — stability analysis of a planar five-link biped. *Journal of Applied Mechanics*, 60:337–343, June 1993.

[14] T. McGeer. Powered flight, child's play, silly wheels, and walking machines. Technical report, Simon Fraser University, Burnaby, British Columbia, Canada, 1989.

[15] T. McGeer. Passive dynamic walking. *The International Journal of Robotics Research*, 9(2):62–82, April 1990.

[16] T. McGeer. Passive walking with knees. In *Proceedings 1990 IEEE International Conference on Robotics and Automation*, pages 1640–1645, Los Alamitos, CA, 1990. IEEE, IEEE.

[17] T. McGeer. Passive dynamic catalogue. Technical report, Aurora Flight Sciences Corporation, 1991.

[18] T. McMahon. Mechanics of locomotion. *International Journal of Robotics Research*, 3(2):4–28, 1984.

[19] M. G. Pandy and N. Berme. Synthesis of human walking: a planar model for single support. *Journal of Biomechanics*, 21(12):1053–1060, 1988.

[20] R. Pratap, S. Mukherjee, and F. C. Moon. Limit cycles in an elasto-plastic oscillator. to appear in Physics Letters, 1992.

[21] S. W. Shaw and P. J. Holmes. A periodically forced piecewise linear oscillator. *Journal of Sound and Vibration*, 90(1):129–155, 1983.

[22] S. W. Shaw and R. H. Rand. The transition to chaos in a simple mechanical system. *International Journal of Non-Linear Mechanics*, 24(1):41–56, 1989.

[23] G. Taga, Y. Yamaguchi, and H. Shimizu. Self-organized control of bipedal locomotion by neural oscillators in an unstable environment. *Biological Cybernetics*, 65(3):147–159, 1991.

[24] M. Vukobratovic, B. Borovac, D. Surla, and D. Stokic. *Scientific Fundamentals of Robotics 7—Biped Locomotion: Dynamics, Stability, Control, and Application.* Communications and Control Engineering Series. Springer-Verlag, Berlin, 1990.

[25] G. T. Yamaguchi. Performing whole-body simulations of gait with 3-D, dynamic musculoskeletal models. In J. M. Winters and S. L-Y. Woo, editors, *Multiple Muscle Systems: Biomechanics and Movement Organization*, chapter 43, pages 663–679. Springer-Verlag, New York, 1990.

[26] F. Zajac and J. M. Winters. Modeling musculoskeletal movement systems: Joint and body-segment dynamics, musculotendinous actuation and neuromuscular control. In J. M. Winters and S. L-Y. Woo, editors, *Multiple Muscle Systems: Biomechanics and Movement Organization*, chapter 8, pages 121–148. Springer-Verlag, New York, 1990.

Appendix

Analytical Approximation to the Jacobian of map f evaluated at fixed point $\mathbf{q}^{\acute{}}$

Stability of periodic motions can be investigated by linearizing the return map about the fixed point $\mathbf{q}^{\acute{}}$ and studying the evolution of small disturbances from the fixed point. The linearization of $\mathbf{f}$ near $\mathbf{q}^{\acute{}}$ is given by

$$\mathbf{q}^{\acute{}} + \Delta\mathbf{f} = \mathbf{f}(\mathbf{q}^{\acute{}} + \Delta\mathbf{q}) \approx \mathbf{f}(\mathbf{q}^{\acute{}}) + \mathrm{D}\,\mathbf{f}(\mathbf{q}^{\acute{}})\Delta\mathbf{q} \tag{40}$$

where $\mathrm{D}\,\mathbf{f}(\mathbf{q}^{\acute{}})$ is the Jacobian matrix, $\mathbf{J}$, called the linearization of the map $\mathbf{f}$ at the fixed point $\mathbf{q}^{\acute{}}$. Since $\mathbf{q}^{\acute{}} = \mathbf{f}(\mathbf{q}^{\acute{}})$, we obtain

$$\Delta^{i+1}\,\mathbf{q}^{+} = \Delta\mathbf{f} \approx \mathbf{J}\Delta^{i}\mathbf{q}^{+} : \tag{41}$$

An asymptotic approximation to the Jacobian of the return map can be obtained as follows. Recall that we have the differential equation of motion between collisions

$$\dot{\mathbf{q}} = \mathbf{g}(\mathbf{q}); \tag{42}$$

subject to the initial condition $\mathbf{q}(0) = {}^{i}\mathbf{q}^{+}$.

We also have the collision transition rule (see equation 8)

$${}^{i}\mathbf{q}^{+} = \mathbf{h}({}^{i}\mathbf{q}^{i}) = \mathbf{L}({}^{i}\mathbf{q}^{i})\,{}^{i}\mathbf{q}^{i} : \tag{43}$$

We define a *collision detection function* 'r' such that a collision occurs when $r(\mathbf{q}^i) = 0$. In our system, the collision detection function is

$$r(\mathbf{q}^i) = \quad ¡ \frac{\cdots}{n}: \tag{44}$$

Assume a fixed point $\mathbf{q}^{\prime}$ of the system exists with corresponding limit cycle trajectory $\mathbf{q}^{\prime}(¿)$. The pre-collision state vector is ${}^{i+1}\mathbf{q}^i = \mathbf{q}^{\prime}(¿^{\prime})$, where $¿^{\prime}$ is the limit cycle time between collisions. So, the collision detection and transition rules give

$$r(\mathbf{q}^{\prime}(¿^{\prime})) = 0 \text{ and } \mathbf{h}(\mathbf{q}^{\prime}(¿^{\prime})) = \mathbf{q}^{\prime}: \tag{45}$$

For a particular system, we need to find the limit cycle trajectory $\mathbf{q}^{\prime}(¿)$ and the time $¿^{\prime}$ between collisions in the limit cycle. See Figure 6 for a schematic illustration of the limit cycle time history.

We wish to study the evolution of a perturbation from the fixed point, just after collision i, $\Delta\mathbf{q} = †\hat{\mathbf{q}}$, where $†$ is small. Henceforth, we shall use a 'hat' ($\hat{}$) to denote perturbations to limit cycle quantities. So, just after a collision, say the i_{th}, the perturbed state of the wheel is

$${}^i\mathbf{q}^+ = \mathbf{q}^{\prime}_0 + †\hat{\mathbf{q}}_0 = \mathbf{q}^{\prime}_0 + †({}^i\hat{\mathbf{q}}^+): \tag{46}$$

The solution to the differential equation between collisions with this perturbed initial condition is some

$$\mathbf{q}(¿) = \mathbf{q}^{\prime}(¿) + †\hat{\mathbf{q}}(¿): \tag{47}$$

As a result of perturbing the fixed point, the limit cycle time between collisions is also perturbed,

$$¿_f = ¿^{\prime} + \Delta¿ = ¿^{\prime} + †\hat{¿}: \tag{48}$$

See Figure 6 for a schematic illustration of the perturbed limit cycle time history. We substitute the perturbed quantities into the governing equation of motion, the collision detection function, and the collision transition rule. We then expand and truncate the resulting expressions to first order in epsilon. We obtain:

1. an expression governing the evolution of a perturbation to the limit cycle from just after a collision to just before the next, (a linear non-autonomous system)

$$\dot{\hat{\mathbf{q}}}(¿) = D\mathbf{g}(\mathbf{q}^{\prime}(¿))\hat{\mathbf{q}}(¿); \tag{49}$$

2. an expression for the perturbation to the time between collisions $\hat{¿}$,

$$\hat{¿} = ¡ \frac{Dr(\mathbf{q}^{\prime}(¿^{\prime}))\hat{\mathbf{q}}^{\prime}(¿^{\prime})}{Dr(\mathbf{q}^{\prime}(¿^{\prime}))\dot{\mathbf{q}}^{\prime}(¿^{\prime})}; \text{ and} \tag{50}$$

3. an expression for the evolution of the perturbation to the limit cycle, through one cycle

$${}^{i+1}\hat{\mathbf{q}}^+ = D\mathbf{h}(\mathbf{q}^{\prime}(¿^{\prime})) \bullet \mathbf{I} ¡ \frac{\dot{\mathbf{q}}^{\prime}(¿^{\prime}) \diamond Dr(\mathbf{q}^{\prime}(¿^{\prime}))}{Dr(\mathbf{q}^{\prime}(¿^{\prime})) \diamond \dot{\mathbf{q}}^{\prime}(¿^{\prime})} \hat{\mathbf{q}}(¿^{\prime}): \tag{51}$$

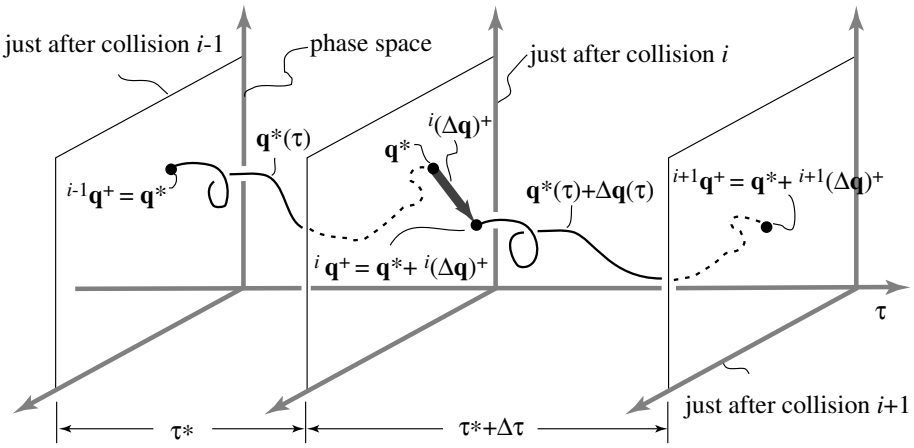

Figure 6: Schematic showing the unperturbed and perturbed fixed point, limit cycle trajectory, and limit cycle period.

Putting these expressions together, we obtain an analytical approximation to the linear map governing the evolution of perturbations from collision to collision as a product of three special matrices

$$^{i+1}\hat{\mathbf{q}}^+ \prime \underbrace{\mathbf{BDE}}_{\mathbf{A}} {}^i\hat{\mathbf{q}}^+ \tag{52}$$

where

$$\mathbf{B} \cdot \mathrm{D}\,\mathbf{h}(\mathbf{q}^{\prime}(\textquestiondown^{\prime})) \text{ and } \mathbf{D} \cdot \mathbf{I} + \frac{\dot{\mathbf{q}}^{\prime}(\textquestiondown^{\prime}) \otimes \mathrm{D}r(\mathbf{q}^{\prime}(\textquestiondown^{\prime}))}{\mathrm{D}r(\mathbf{q}^{\prime}(\textquestiondown^{\prime})) \otimes \dot{\mathbf{q}}^{\prime}(\textquestiondown^{\prime})} : \tag{53}$$

The matrix $\mathbf{E}$ can be obtained by integrating equation 49 with arbitrary initial condition $^i\hat{\mathbf{q}}^+$ forward up to time $\textquestiondown^{\prime}$,

$$\hat{\mathbf{q}}(\textquestiondown^{\prime}) \prime \mathbf{E}\,{}^i\hat{\mathbf{q}}^+ : \tag{54}$$

The three matrices comprising the approximation to the Jacobian, $\mathbf{A} = \mathbf{BDE}$, have the following interpretations. Matrix $\mathbf{B}$ is the linearization of the collision transition map at the fixed point of interest. Matrix $\mathbf{E}$ maps the disturbances or perturbations to the limit cycle from just after one collision to just before the next, *not* accounting for any small changes in the time of collision. Matrix $\mathbf{D}$ introduces the necessary correction due to the fact that the time of collision is, in fact, slightly altered due to the disturbances.

In order to obtain this approximate Jacobian, we need to find the limit cycle trajectory $\mathbf{q}^{\prime}(\textquestiondown)$ and the limit cycle time between collisions $\textquestiondown^{\prime}$. As we do not have explicit solutions for these quantities, we use approximate methods to obtain them (a perturbation expansion in $\dagger$, in this case).